Optics Letters

Phase-interfacial stimulated Raman scattering generated in strongly pumped water

Hong Yuan,[1,2] Baodong Gai,[1,2] Jinbo Liu,[1,*] Jingwei Guo,[1] Hui Li,[1] Shu Hu,[1] Liezheng Deng,[1] Yuqi Jin,[1] and Fengting Sang[1]

[1]Key Laboratory of Chemical Lasers, Dalian Institute of Chemical Physics, Chinese Academy of Sciences, Dalian 116023, China
[2]University of Chinese Academy of Sciences, Beijing 100049, China
*Corresponding author: liujinbo@dicp.ac.cn

Received 30 May 2016; revised 23 June 2016; accepted 23 June 2016; posted 23 June 2016 (Doc. ID 267295); published 14 July 2016

We have observed unusual blue-shifted radiations in water pumped by a strong 532-nm nanosecond laser. Properties including divergence, polarizations, and pulse shapes of the unusual radiations are measured and compared with those of the regular stimulated Raman scattering (SRS) in water. The unusual radiations are attributed to the parametric anti-Stokes SRS that occurs on the interface of water and ionization plasma (or gas) formed in the laser-induced breakdown of water.

OCIS codes: (240.0240) Optics at surfaces; (240.4350) Nonlinear optics at surfaces; (290.5910) Scattering, stimulated Raman; (290.5900) Scattering, stimulated Brillouin.

http://dx.doi.org/10.1364/OL.41.003335

SRS has achieved numerous applications in wavelength conversion and physical properties probing of dense media since the invention of the laser [1–5]. Recently, unusual SRS in water has received great interest from researchers. For example, Men *et al.* report the SRS evidence of transient generation of ice-VII, ice-VIII, and ice-X [6,7] in laser-induced shockwave experiments in water. The tens of GPa giant pressure [8–11] of the shockwave is responsible for the water-ice conversion. Research about improving SRS efficiency in water/solutions through novel mechanisms has also received interests. Ganot *et al.* [12] report a Stokes efficiency of ~35% at a pump energy of 120 mJ/pulse in low temperature water. Low temperature can suppress the competing stimulated Brillouin scattering (SBS) process in water and improve the SRS conversion of the pump beam. The same group also reports a high efficiency SRS in a saturated $NaNO_3$ solution with 12% and 4% efficiencies in generating first and second Stokes outputs, respectively [13]. SRS on water surfaces in air has attracted a lot of interests recently. Yui has used a moveable focal point of a 532-nm picoseconds laser irradiates the water vertically to examine the generated backward SRS radiations [14]. A peak at 3000 cm^{-1} beside the normal 3400 cm^{-1} peak appears when the focal point is moved to the surface of water. The 3000 cm^{-1} peak is considered to be related to the plasma electrons at the water surface. Li *et al.* have also given similar backward SRS results, a 3000 cm^{-1} peak appears only when the focal point of the pump laser is on the water surface. The 355-nm nanosecond laser's focal point irradiates the water horizontally [15]. A model of bilayer of water molecules with ordered structure on the surface of the plasma plume is proposed, and the bilayer is considered to be related to the 3000 cm^{-1} SRS peak. The Raman properties of water/(other material) interfaces can disclose the interface-structure; however, studying the Raman properties of interfaces remains challenging. We find the parametric anti-Stokes generation in water SRS is a powerful tool to examine the water/plasma (or gas) interfaces formed in water. Several unusual anti-Stokes bands are reported here and explained with an interfacial SRS model.

The experimental setup is illustrated in Fig. 1. A frequency doubled *Q*-switched Nd:YAG laser (Powerlite-9020, Continuum; 532 nm, 20 Hz, full-width-half-magnitude pulse width 10 ns) pumps water to generate SRS. A beam isolator [a polarized beam splitter cube (PBS) and a $\lambda/4$ waveplate at 532 nm ($\lambda/4$ WP)] isolates the backward SBS radiation. Distilled water is used in a 10-cm-length quartz cell. A lens (L1, focal length $f = 50.8$ mm) focuses the 532-nm beam

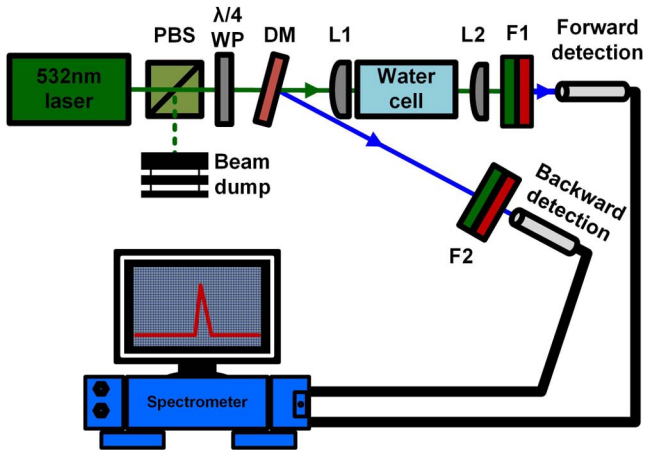

Fig. 1. Illustration of the experimental setup for water SRS generation and measurement.

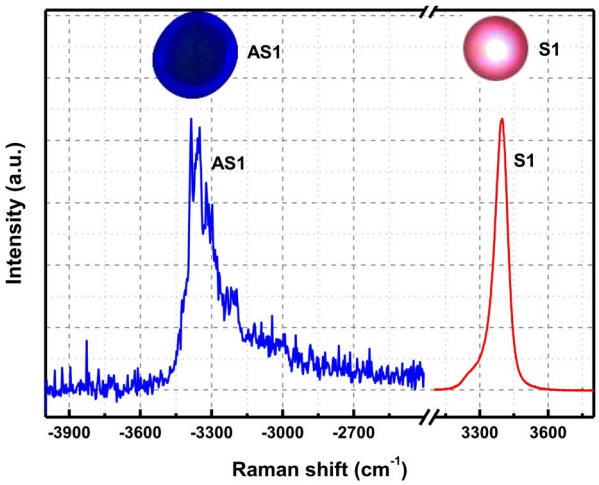

Fig. 2. Averaged Raman shifts of the forward radiations and their corresponding beam profiles.

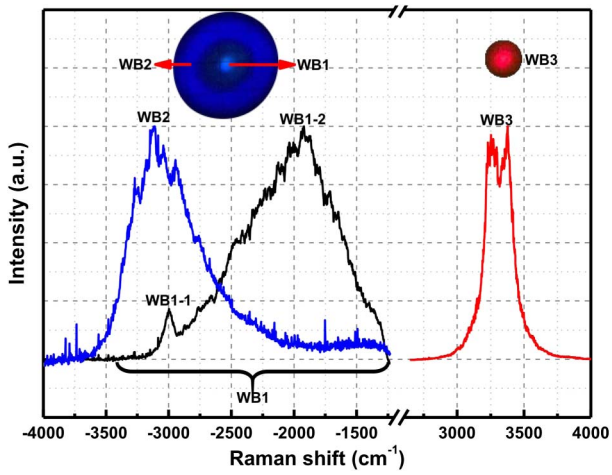

Fig. 3. Averaged Raman shifts of the backward radiations and their corresponding beam profiles.

into water. The forward radiations are collimated by a lens (L2, $f = 100$ mm). The backward radiations are separated using a 500-nm long-pass dichroic mirror (DM) which can attenuate red radiations. Beam profiles are recorded with a camera. Spectra of the radiations are measured with spectrometers (iHR320, HORIBA; FHR1000, HORIBA), and laser-filters (F1, F2) are used when necessary. Radiation polarizations are measured with a zero-order $\lambda/4$ waveplate at 532 nm and a polarization plate. Broad peaks are shown in spectra of the radiations. For convenience, they are referred to as "WB"s (wave-bands). All spectra of the radiations are given in wavenumber (cm^{-1}). All measurements are carried out with pump pulse energy of 100 mJ ($\sim 1.4 \times 10^{12}$ W $\cdot$ cm^{-2} at focal point) unless there is a special illustration.

Normal SRS radiations (Fig. 2) appear in the forward direction. A concentric red spot and blue circle are observed. The red spot owns the Raman peak at $\sim$3400 cm^{-1} (frequency shift from the 532 nm) (S1), and the blue circle owns ~ -3400 cm^{-1} (AS1). These Raman shifts are well in accordance with the normal Raman spectra of liquid-state water [16]. The blue circle implies a conical radiation, which is derived from the color-dispersion caused noncollinear phase matching process in the parametric generation [17] of the anti-Stokes curve.

Spectra in Fig. 3 show unusual frequencies. When the backward SBS beam is filtered away, on screen at the place of SBS spot a blue band (WB1) and a red band (WB3) are visible. A larger blue ring (WB2) is also noticed. The WB1 band is composed with a peak centered at ~ -3000 cm^{-1} (WB1-1) and a peak centered at ~ -2000 cm^{-1} (WB1-2). The WB3 band is similar to the Stokes emission in Fig. 2, but owns a split form. The WB2 has a broadband ($\sim$500 cm^{-1}) width centered at ~ -3000 cm^{-1}. These WBs do not match the shift frequencies in normal Raman spectra of liquid water [16].

Time-resolved peak-intensity measurements of the backward radiations are carried out and shown as Fig. 4 (measured using the time-gate function of an intensified charge couple device). SBS and all WBs peaks recorded in Fig. 3 own their existing time range inside the 532-nm pump pulse. The tail-like ending shape of WB1-1 is caused by a baseline elevation from a spectra overlapped, broadband and flat early-stage

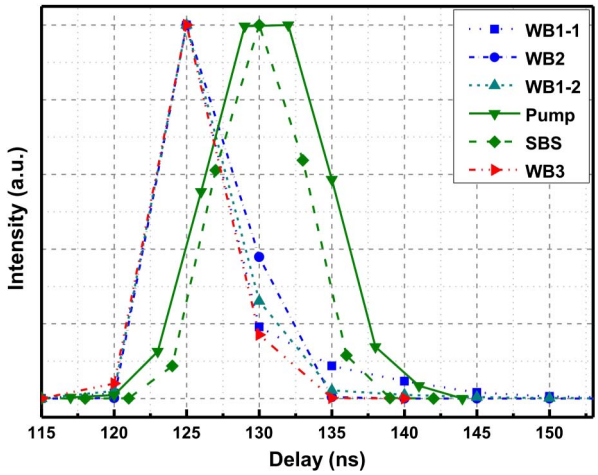

Fig. 4. Time resolved intensities of the pump pulse and backward radiations in this work.

plasma fluorescence [18]. These time features prove the backward radiations are derived from fast processes with at least nanosecond grade speed.

To determine physics sources of the radiations in Fig. 3, a relevancy test is carried out between the blue-shifted bands (including WB1 and WB2) and the red-shifted bands (WB3) in the backward direction. When the pump pulse energy is set to the range of $\sim$20 – 40 mJ ($\sim 3 \times 10^{11} - 6 \times 10^{11}$ W $\cdot$ cm^{-2} at focal point) WB1, WB2, and WB3 become unstable, and peaks begin to flicker while the backward SBS is stably generated. Results show the blue-shifted bands (WB1 and WB2) only appear together with the WB3 from pulse to pulse, while the WB3 can appear alone. This relevancy is quite similar to that of the well-known controllable parametric anti-Stokes spectroscopy, CARS (coherent anti-Stokes Raman scattering) [19]. If the Stokes laser is blocked, the CARS signal disappears immediately. In addition, all radiations recorded in Fig. 3 own identical circular polarization with the pump beam, and own fast speed shown in Fig. 4. The WB1 and WB2

disappear together with the backward SBS and WB3 when the laser focal point in water is removed by a rough rod placed at the position of the focal point. When the water is changed to heavy water (deuterium oxide), the WBs still exist with similar beam profiles. WB1-1, WB1-2, WB2, and WB3 shift to centers at ~ – 2300, –1800, –2200 and 2400 cm^{-1}, respectively. We found only a parametric anti-Stokes process involving the backward SBS and the bright WB3 as light sources can explain the generation and above properties of WB1 and WB2 [20].

WB3 is generated at the focal point. A splitting peak similar to WB3 in this work is reported by Yui [14,21]. That result is obtained with a picosecond laser. The splitting is considered to be related to a hydrated electron generated by laser-induced breakdown. The hydrated electron can be seen as a small cluster, and the cluster owns weaker O-H bands and lower O-H vibration frequency. The coexisting of normal and lower frequency leads to a split SRS Stokes peak. A quantum-chemistry calculating is also carried out by Yui to verify the vibration frequency shift [22]. Addition of the electron scavenger agent H_2O_2 changes the backward Stokes spectrum to a nearly regular water Raman spectrum. We find WB3 is broad enough (from 3400 cm^{-1} to less than 2000 cm^{-1}) to be a Stokes source to generate parametric anti-Stokes radiations.

The circle-shaped WB2 owns much larger divergence than the pump laser, backward SBS beam, WB1 and WB3. This means WB2 originates at the place nearer to the inlet optical window of the quartz cell than the focal point, according to the "reversible light-path" principle in geometrical optics. The distance from the area emitting WB2 to the focal point is estimated to be approximately 0–25 mm according to the divergence of WB2 and the refractivity index of water. At the corresponding area tiny bubbles can be seen. Due to the 20 Hz repetition frequency of the pump laser, the bubbles are continuously generated from the focal point, moving outward and accumulating around the focal point as Fig. 5(a). Inside the bubble should be stable gases such as H_2 and O_2 from water dissociation. Since WB2 shows Raman frequency

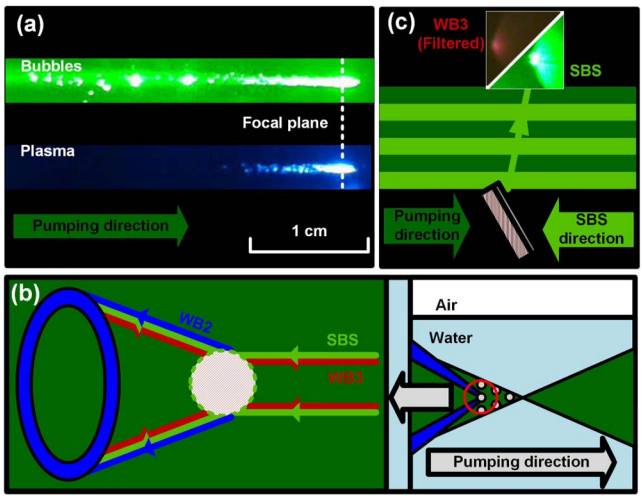

Fig. 5. Schematic illustration on the generation of the broadband WB2. (a) Bubbles and plasma images around the focal point in water. (b) Amplified local showing the SRS generated on the interface of a bubble. (c) The incomplete phase-conjugating property of backward SBS and WB3 shown using a mirror partly wedged into the main optical path before the water cell.

different from bulk water, the water-gas interfaces of bubbles are deduced to be related to the generation of WB2. According to the circle-shape of WB2, a WB2 generation model is illustrated as Fig. 5(b). Bubbles generated from former pulses can contribute to later WB2 pulses. SBS is known as a phase-conjugating radiation which "retrospects" the path of its pump beam. If so, bubbles cannot be illumined in the way of Fig. 5(b). A mirror-wedge test illustrated in Fig. 5(c) proves the SBS and WB3 are not precise phase-conjugating beams of the pump beam. So it is reasonable the SBS and WB3 beam can at least partly illumine the bubbles in the reverse direction of pump beam to generate WB2 as shown in Fig. 5(b).

From bulk water to the water-gas interface, water molecules experience a gradually change of hydrogen-bond network instead of a sudden change. The water-air interface is continually studied, the most popular model to describe the O-H bonds including dangling O-H bond in air (~3700 cm^{-1}) and O-H bonds in the hydrogen-bond network (~3100 – 3400 cm^{-1}) [23]. Here the –3000 cm^{-1} frequency-shift probably mean a frequency-selecting Raman stimulation on the interface caused by the Raman activity difference of O-H bonds. The result of WB2 shows high sensitivity and extends the theories of Yui [14] and Li [15] to a much lower laser power density (from 1×10^{11} to 1×10^{9} $W \cdot cm^{-2}$). The different interfaces on different sizes of bubbles are thought to compose the large averaged bandwidth around 3000 cm^{-1} of WB2.

It is a challenge to assign the WB1 SRS band to a proper vibration process. The deviation between the spectra of WB1 and bulk water SRS is also significant. The WB1 shows a solid spot profile with size similar to WB3. This means an unusual colinear phase matching characteristic in the parametric generation of WB1. A similar phenomenon is reported in [24] and a theory of self-induced phase-matching under high pump power at focus is introduced to explain it. We have noticed that with the best sensitivity of our equipment, we can only record WB1 above the ionization limit of water. The WB1-1 has similar Raman frequency shift to WB2, but owns narrower width than WB2. WB1-1 is possibly generated from cold bubbles that stay at the focal point. The unusual shift of WB1-2 is possibly related to a shifted O-H bending vibration as a result of the high-pressure environment [25] at the interface of water and expanding laser-induced-plasma. Under a large range of pump energy (from detection limit to ~100 mJ/pulse), the band does not show significant deformation. Measurements with higher sensitivity and higher resolution in time will help to disclose these phenomena about WB1 better.

Unusual radiations at 460 nm (~ – 3000 cm^{-1}) and 480 nm (~ – 2000 cm^{-1}) are recorded in the backward radiations of water under a strong pump. The phenomena are attributed to parametric anti-Stokes SRS derived from the water-gas or water-plasma interface formed in the laser induced breakdown of water. The parametric anti-Stokes method shows high sensitivity and may be quite useful in detecting Raman properties of kinds of interfaces.

Funding. National Natural Science Foundation of China (NSFC) (11304311, 11475177).

REFERENCES

1. W. Wang, M. Gong, Q. Zhao, Z. Hu, and C. Fu, Opt. Express **18**, 2655 (2010).

2. L. Zhang, H. Jiang, S. Cui, J. Hu, and Y. Feng, Laser Photon. Rev. **8**, 889 (2014).
3. T. Naito, T. Tanaka, K. Torii, N. Shimojoh, H. Nakamoto, and M. Suyama, in *Optical Fiber Communication Conference and Exhibition (OFC)* (2002), 116.
4. J. Moros, J. A. Lorenzo, K. Novotný, and J. J. Laserna, J. Raman Spectrosc. **44**, 121 (2013).
5. B. H. Hokr, J. N. Bixler, G. D. Noojin, R. J. Thomas, B. A. Rockwell, V. V. Yakovlev, and M. O. Scully, Proc. Natl. Acad. Sci. USA **111**, 12320 (2014).
6. Z. Men, W. Fang, D. Li, Z. Li, and C. Sun, Sci. Rep. **4**, 4606 (2014).
7. Z. Men, Z. Li, M. Zhou, G. Lu, B. Zou, Z. Li, and C. Sun, Phys. Rev. B **85**, 092101 (2012).
8. K. R. Hirsch and W. B. Holzapfel, J. Chem. Phys. **84**, 2771 (1986).
9. I.-M. Chou, J. G. Blank, A. F. Goncharov, H.-K. Mao, and R. J. Hemley, Science **281**, 809 (1998).
10. M. Song, H. Yamawaki, H. Fujihisa, M. Sakashita, and K. Aoki, Phys. Rev. B **68**, 014106 (2003).
11. M. Abebe and G. E. Walrafen, J. Chem. Phys. **71**, 4167 (1979).
12. Y. Ganot, S. Shrenkel, B. D. Barmashenko, and I. Bar, Appl. Phys. Lett. **105**, 061107 (2014).
13. Y. Ganot and I. Bar, Appl. Phys. Lett. **107**, 131108 (2015).
14. H. Yui, Anal. Bioanal. Chem. **397**, 1181 (2010).
15. Z. Li, H. Li, W. Fang, S. Wang, C. Sun, Z. Li, and Z. Men, Opt. Lett. **40**, 3253 (2015).
16. G. R. Medders and F. Paesani, J. Chem. Theory Comput. **11**, 1145 (2015).
17. H. Zeiger, P. Tannenwald, S. Kern, and R. Herendeen, Phys. Rev. Lett. **11**, 419 (1963).
18. A. De Giacomo, M. Dell'Aglio, and O. De Pascale, Appl. Phys. A **79**, 1035 (2004).
19. R. Begley, A. Harvey, and R. Byer, Appl. Phys. Lett. **25**, 387 (1974).
20. R. Boyd, *Nonlinear Optics* (Academic, 2003).
21. H. Yui and T. Sawada, Phys. Rev. Lett. **85**, 3512 (2000).
22. H. Yui, T. Nakajima, K. Hirao, and T. Sawada, Anal. Sci. **24**, 111 (2008).
23. Q. Du, R. Superfine, E. Freysz, and Y. R. Shen, Phys. Rev. Lett. **70**, 2313 (1993).
24. K. Hakuta, M. Suzuki, M. Katsuragawa, and J. Z. Li, Phys. Rev. Lett. **79**, 209 (1997).
25. R. J. Hemley, Annu. Rev. Phys. Chem. **51**, 763 (2000).